Acta Geochim (2017) 36(2):166–180
DOI 10.1007/s11631-017-0143-9

ORIGINAL ARTICLE

Geochemistry, petrogenesis and tectonic significance of the late Triassic A-type granite in Fujian, South China

Dawei Cai[1,2] · Jingyu Zhao[1,2] · Yong Tang[1] · Hui Zhang[1] · Yunlong Liu[1,2] · Zhenghang Lv[1]

Received: 8 September 2016 / Revised: 11 December 2016 / Accepted: 18 January 2017 / Published online: 24 March 2017

Abstract The late Permian–Triassic granites in southeastern China have important tectonic significance for the evolution of South China. Here, we present the detailed geochronological, geochemical and petrological analyses for the Jinlongyan (JLY) granite in northwest Fujian Province, southeast China. LA–ICP–MS zircon U–Pb dating yielded a weighted average $^{206}Pb/^{238}U$ age of 224.1 ± 3.3 Ma. The granite is mainly comprised of K-feldspar, plagioclase, quartz, biotite and minor amphibole. It is characterized by enrichments in Rb, Th, REEs (total REE = 295.1–694.3 ppm), and HFSEs (e.g., Zr = 289–520 ppm, Hf = 9.3–15.0 ppm, Y = 36.2–68.2 ppm) but depletions in Ba, Sr, Eu and Ti. The granite is metaluminous to weakly peraluminous and show a clear A-type granite geochemical signature with high SiO_2 (70.89 wt%–75.76 wt%), total alkalis ($Na_2O + K_2O$ = 7.51 wt% –8.72 wt%), Ga/Al ratios (10000 Ga/Al = 2.72–3.43). In-situ zircon Hf isotope analysis shows their $\varepsilon_{Hf}(t)$ values ranging from −7.2 to −3.2, with Mesoproterozoic T_{2DM} ages (1308–1525 Ma). Whole-rock Nd isotope data show their $\varepsilon_{Nd}(t)$ values in the range of −9.5 to −9.1 and yield paleoproterozoic T_{DM} ages (1606–1985 Ma). These characteristics indicate that the JLY A-type granite magma was formed by the partial melting of Meso-Paleoproterozoic crust rocks in the Cathaysia Block. Our study of the JLY A-type granite, together with other Triassic A-type granites in South China, defines an extensional environment in the late Triassic which probably was caused by the collision of the South China Block with Indochina Block.

Keywords A-type granite · U–Pb dating · Sr–Nd–Hf isotope · Late Triassic · Fujian Province

1 Introduction

The South China Block (SCB) is bounded to the north by the Qinling–Dabie–Sulu Orogen (Zhang 1997; Meng and Zhang 1999) and to the south by the Jinshajiang-Ailaoshan-Songma (Song Chay) Orogen (Faure et al. 2014). The eastern margin of the block extends to the continent-ocean boundary with the South China Sea. The SCB is composed of two subblocks, with the Yangtze in the northwest and the Cathaysia in the southeast (Fig. 1). Cathaysia is characterized by large exposure of the Mesozoic granitic rocks (~28.3% of the land surface on five southeastern provinces; Zhou et al. 2006) that are conventionally separated into the Indosinian (mainly Triassic), Early Yanshanian (Jurassic) and Late Yanshanian (Cretaceous) intrusives. The Indosinian intrusive rocks are the least voluminous and limited to the interior of Cathaysia.

Mesozoic granites have attracted the interests over the last decades because of their economically significant mineralization. These granites develop extensively in response to the tectonic evolution of the region so that their petrogenesis is important for understanding the Mesozoic tectonic evolution of the block (Jahn 1974; Chen and Jahn 1998; Zhou and Li 2000; Li and Li 2007; Wang et al. 2007b; Hsieh et al. 2008; Pirajno et al. 2009). Various tectonic regimes have been proposed by different researchers. Ren (1964, 1991) and Holloway (1982) advocated that the westward subduction of the Pacific plate dominated the Mesozoic tectonic evolution

✉ Yong Tang
tangyong@vip.gyig.ac.cn

[1] Key Laboratory for High Temperature and High Pressure Study of the Earth's Interior, Institute of Geochemistry, Chinese Academy of Sciences, Guiyang 550081, China

[2] University of Chinese Academy of Sciences, Beijing 100049, China

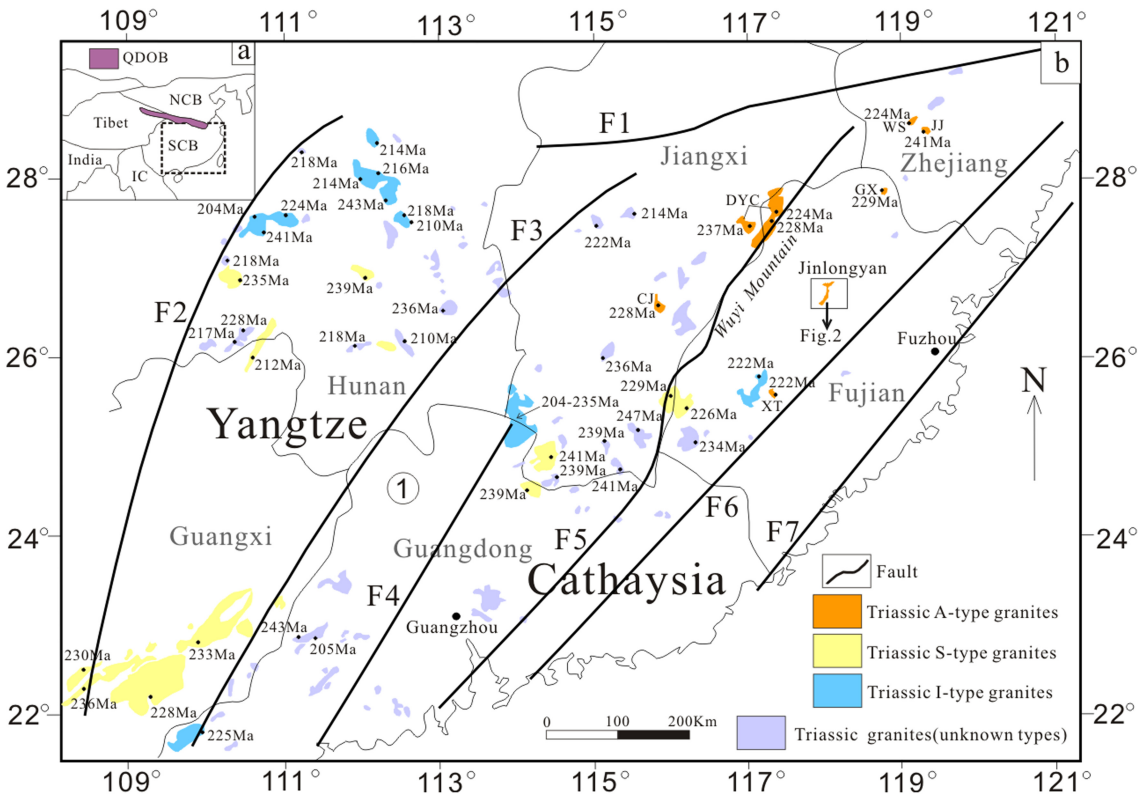

Fig. 1 Schematic map showing the distribution of the Triassic granites in the SCB. *SCB* South China Block, *QDOB* Qinling-Dabie Orogenic Belt, *NCB* North China Block, *YC* Yangtze Block, *IC* Indochina Block. Granites; *DYC* Dayinchang A-type granite (Wang et al. 2013a); *WS* Wengshan A-type granites (Sun et al. 2011); *JJ* Jingju A-type granites (Gao et al. 2014); *GX* Gaoxi A-type granites (Zhao et al. 2013); *CJ* Caijiang A-type granites (Zhao et al. 2013); *XT* Xiaotao aluminous A-type granites (Wang et al. 2007a). *F1* Jiangshan-Shaoxing Fault; *F2* Jinxian-Anhua Fault; *F3* Binxian-Linwu Fault; *F4* Sishui-Wuchuan Fault; *F5* Heyuan-Guangfeng Fault; *F6* Zhenhe-Dapu Fault; *F7* Changle-Nan'ao Fault

of the SCB. Hsü et al. (1990) proposed a model of the Triassic Alps-type collision, with an assumption that the pre-collision "Banxi ocean and Banxi ophiolite mélange" had been developed within the SCB. Chen et al. (1994) also attempted to expand this model further. Wang et al. (2005) proposed a transtensional tectonic regime which was genetically related to the oblique subduction of proto-Pacific plate underneath South China. Li and Li (2007) invoked a flat-slab subduction model of the Paleo-Pacific plate since the Permian to explain the broad deformation and granitic magmatism. Wang et al. (2007b) advocated that the Indosinian orogeny in the SCB was resulted from intracontinental convergence during the final assembly of Pangea, by which the less competent SCB was squeezed between the more competent NCB and Indochina Block (e.g. Liang and Li 2005; Zhang et al. 2011). Lepvrier et al. (2004, 2008), Zhou et al. (2006) and Shu et al. (2008) proposed that Indosinian magmatism was caused by northward subduction and collision of the Indochina Block with the SCB in response to closure of the Paleo-Tethys ocean.

So far there is no consensus on the tectonic regimes due to the different recognition of the distribution and petrogenesis of the relevant Mesozoic igneous rocks. Fujian Province, which is situated in the southeastern part of South China, is a key area for understanding the tectonic evolution of the region. This paper reports the discovery of a late Triassic A-type granitic pluton in northwestern Fujian, South China. A-type granites are particularly important because they may indicate an extensional tectonic environment on regional scale (Loiselle and Wones 1979; Whalen et al. 1987; Eby 1992; Turner et al. 1992; Bonin 2007). Petrography, major and trace element geochemistry, and Sr–Nd–Hf isotopic compositions and in situ zircon U–Pb ages of the Jinlongyan granitic pluton have been carried out. These results will be used to constrain their ages, petrogenesis and magma sources, and thus provide key evidences for understanding the tectonic setting of the SCB during the late Triassic.

2 Geological setting

The stratigraphic succession of northwest Fujian can be grouped into five major, unconformity bounded sequences: (1) Precambrian basement; (2) Cambrian through Middle

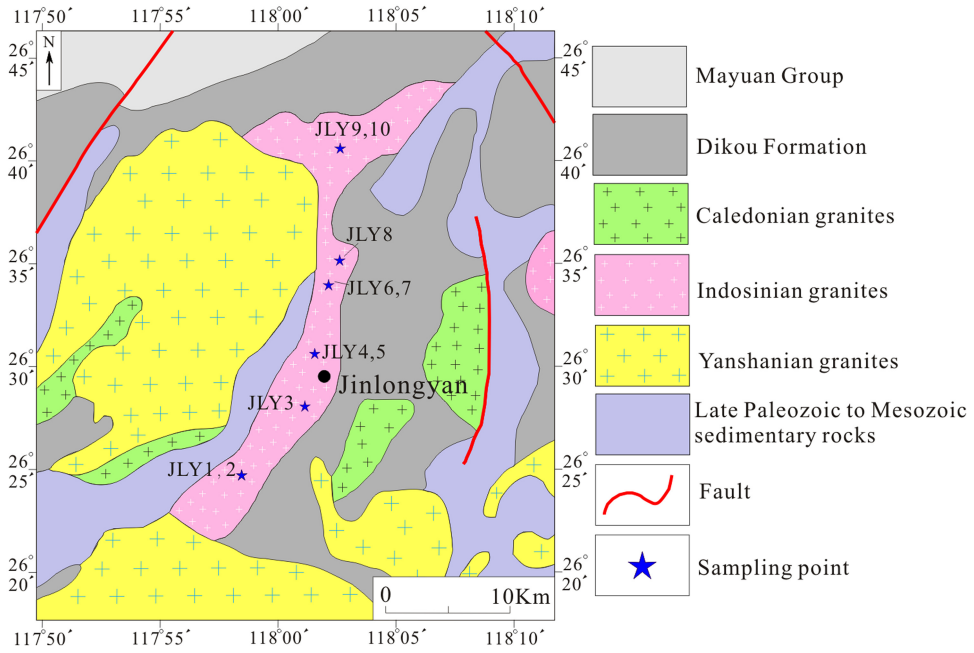

Fig. 2 Simplified geological map of the Jinlongyan granite (modified after Yang et al. 1987)

to Late Ordovician pelagic to hemipelagic sediments; (3) Late Devonian to Early Triassic platform sequence; (4) Early to Middle Jurassic syn-tectonic foreland basin deposits; (5) Late Jurassic to Late Cretaceous volcanic assemblage and terrestrial basin deposits (Chen 1999). In the Cathaysia Block, the basement is dominantly 1.9–1.8 Ga sedimentary rocks and Neoproterozoic to lower Paleozoic metamorphic rocks (Yu et al. 2005). Subsequently, the occurence of continuous sedimentation in the SCB lasted 400 million years (Wang and Li 2003). Platform-type strata started with transgressive Late Devonian to Early Carboniferous conglomerates and sandstones followed by Middle Carboniferous to Early Permian shallow-marine carbonates (Fujian Bureau of Geology 1985). From the Late Permian to Early Triassic, the shallow-marine strata gave way to more pelagic sediments of siliciclastic facies and flysch-like sequences of siltstone and carbonate turbidites and hemipelagic shales (Fujian Bureau of Geology 1985).

The Mesozoic magmatism in the Cathysia block was mainly granitic magmatism with a planar distribution feature, and majority of these granites has been classified as peraluminous granites (Zhou et al. 2006). There was also a small amount of syenite in Jiangxi, Zhejiang and Fujian (Wang et al. 2005; He et al. 2010; Zhu et al. 2013) and mafic rocks in Hunan and Hainan Province (Guo et al. 1997; Dai et al. 2008; Tang et al. 2013). NE-trending fault zones are well developed in the whole of Cathaysia (Fig. 1). From east to west, major regional structures in the SCB are the Changle-Nan'ao, Zhenhe-Dapu, Heyuan-Guangfeng, Sishui-Wuchuan, Binxian-Linwu, Jinxian-Anhua fault zones (Fig. 1). The Changle-Nan'ao fault zone appears to have controlled the emplacement of late Cretaceous alkaline or A-type granites in eastern Fujian (Xu et al. 1999). In Cathaysia, the Triassic granites occur primarily to the west of the Zhenhe-Dapu fault.

3 Petrology

The Jinlongyan (JLY) granitic pluton is located in the northwest part of Fujian Province, northeastern Cathaysia Block, SE China (Fig. 1) and occurs as an banded shape with an outcrop area of approximately 78 km^2. The long axis of the pluton trends approximately N–NE, and a series of Yanshanian granitic intrusions crop out around the pluton. The width and length of the pluton is approximately 1–5 and 40 km, respectively. The JLY pluton is mainly enclosed by the Neoproterozoic Dikou Formation to the north and east, and by the Devonian Nanjing Group to the west (Fig. 2). The Neoproterozoic Dikou Formation mainly comprises of fine-grained amphibolite facies garnet- and sillimanite-bearing biotite gneiss, schist and quartzit. SHRIMP zircon U–Pb data indicate that the Dikou Fromation formed later than 0.8 Ga and the metamorphic age should be younger than 604 Ma (Wan et al. 2007). The Devonian Nanjing Group is clastic sedimentary rocks whose lithology is mainly siltstones (Fujian Bureau of Geology 1985). However, isotopic age data of the Nanjing Group are lacking. Folds and faults are also abundant in the study area. The folds are mostly developed in the metamorphic basement, with a predominant N-NE strike, and there are several groups of faults that have destroyed the cover and the basement to different degrees.

Samples investigated in this study were collected from fresh outcrops. The major rock type of the JLY granitic pluton is fine- to medium-grained alkali-feldspar granite with massive structure. The JLY pluton displays a rather consistent mineralogy, and is mainly composed of K-feldspar (35 vol%–45 vol%), plagioclase (20 vol%–30 vol%), quartz (30 vol%–40 vol%) and biotite (3 vol%–5 vol%), occasionally associated with minor amphibole. They also contain diverse accessory minerals including magnetite, titanite, apatite, zircon and monazite. K-feldspar is mainly microcline and orthoclase with 0.5–3 mm in diameter, and commonly shows microcline texture and tartan twinning. Plagioclase is subhedral to euhedral and mostly consist of oligoclase. It occasionally alters to kaolinite and sericite in some locations. Quartz mainly forms aggregates of large phenocrysts. Biotite crystals are found along the boundary of K-feldspar and quartz, and are euhedral to subhedral, strongly pleochroic, and most have been subjected to chloritization of varying degrees.

4 Analytical methods

Analyses for major and trace elements were carried out in ALS Chemex (Guangzhou) Co Ltd. Major oxides were determined by using wavelength-dispersive X-ray fluorescence spectrometry after fusing by lithium tetraborate with analytical deviations of less than 1%. Loss on ignition (LOI) was obtained through heating the sample powder at 1100 °C for 1 h. Trace elements of rocks were analyzed by using inductively coupled plasma mass spectrometry (ICP-MS) after HNO_3 + HF digestion of about 40 mg sample powder.

Zircon grains were separated from sample JLY1 through crushing, conventional magnetic and heavy liquid separation methods followed by hand picking under a binocular microscope. Cathodoluminescence (CL) images of the zircon grains were photographed for investigating the structure and morphology of the zircon grains and selecting spots for U–Pb dating and Lu–Hf analyses. In-situ zircon U–Pb dating was performed in the State Key Laboratory of Continental Dynamics, Northwest University, Xi'an, by using laser ablation inductively coupled plasma mass spectrometry (LA–ICPMS) technique which enables zircon U–Pb dating and zircon trace element analyses at the same time. The laser ablation system was a GeoLas 200 M (Lambda Physik and MicroLas, Germany) equipped with an Agilent 7500a ICP-MS. Analyses were carried out with a beam diameter of 30 μm, ablation depth of 20–40 μm, laser frequency of 10 Hz with an energy of 34–40 mJ, background acquisition of 30 s and signal acquisition of 60 s. Helium was used as carrier gas to transport the ablated sample into the ICP-MS. Zircon 91500 was used as an external standard to normalize isotopic discrimination, and NIST610 were used as internal standards to calibrate and normalize the concentrations of U, Th and Pb, respectively. Isotopic ratios of U–Th–Pb were calculated using ICPMS Data Cal (V4.6) (Liu et al. 2008, 2010), and the U–Pb ages of the samples were calculated using the ISOPLOT program (Ludwig 2003). Correction of common Pb was achieved according to the method of Andersen (2002). The uncertainty of individual analyses is reported with 1σ and the weighted mean $^{206}Pb/^{238}U$ age was calculated at the 2σ level.

In-situ Hf isotope analysis was conducted at the state Key Laboratory of Geological Processes and Mineral Resources, China University of Geosciences in Wuhan, by using a Neptune Plus MC-ICP-MS (Thermo Fisher Scientific, Germany) in combination with a Geolas 2005 excimer ArF laser ablation system (Lambda Physik, Göttingen, Germany). The energy density of laser ablation used in this study was 5.3 J/cm^2. All data were acquired on zircon in single spot ablation mode at a spot size of 44 μm in this study. Each measurement consisted of 20 s of acquisition of the background signal followed by 50 s of ablation signal acquisition. Detailed operating conditions for the laser ablation system and the MC–ICP–MS instrument and analytical method are the same as description by Hu et al. (2012). Time-dependent drifts of Lu–Hf isotopic ratios were corrected using a linear interpolation according to the variations of 91500 and GJ-1. To check the data quality, 91500 and GJ-1 were re-analyzed as unknowns. The obtained $^{176}Hf/^{177}Hf$ ratios are 0.282295 ± 0.000027 ($n = 14$, 2σ) for 91500, and 0.282734 ± 0.000015 ($n = 16$, 2σ) for GJ-1. These results are in good agreement with the recommended $^{176}Hf/^{177}Hf$ ratio within 2σ (0.2823075 ± 58, 2σ; 0.282015 ± 19, 2σ) (Griffin et al. 2006). A decay constant for ^{176}Lu of 1.865×10^{-11} year^{-1} (Scherer et al. 2001) and the present-day chondritic ratios of $^{176}Hf/^{177}Hf = 0.282772$ and $^{176}Lu/^{177}Hf = 0.0332$ (Blichert-Toft and Albarède 1997) were adopted to calculate the initial values of $^{176}Hf/^{177}Hf$ and $\varepsilon_{Hf}(t)$. Depleted mantle Hf model ages were calculated from the measured $^{176}Lu/^{177}Hf$ and $^{176}Hf/^{177}Hf$ ratios of the zircons assuming a present-day $^{176}Hf/^{177}Hf$ ratio of 0.283250 and a $^{176}Lu/^{177}Hf$ ratio of 0.0384 for the depleted mantle (Griffin et al. 2002). The average crustal $^{176}Lu/^{177}Hf$ value of 0.015 was adopted to calculate the two-stage model ages (T_{2DM}) (Griffin et al. 2002). Off-line selection and integration of analytic signals, and mass bias calibrations were performed using ICPMSDataCal (V4.6) (Liu et al. 2008, 2010).

For Sr and Nd isotopic analyses, about 100 mg of whole-rock powder was dissolved in the same way as for the trace element analysis. Complete separation of Sr was achieved by a combination of cation-exchange chromatography in H^+ form and pyridinium form with the

DCTA complex. Nd was then separated from the REE fractions by cation-exchange resin using HIBA as eluent. The details of separation procedures and mass spectrometry can be found in Pu et al. (2004, 2005). The separated Sr sample was dissolved in 1 N HCl and then loaded with TaF_5 solution onto W filament. The separated Nd sample was dissolved in 1 N HCl and then loaded with H_3PO_4 solution onto Re double-filament. Determination of Sr and Nd isotopic composition was carried out by a Finnigan MAT Triton TI TIMS at State Key Laboratory for Mineral Deposits Research, Nanjing University. The NBS-987 Sr standard gave an average value of 0.710260 ± 6 (n = 10, 2σ) in this study. The JNDi-1 Nd standard gave an average value of 0.512118 ± 5 (n = 15, 2σ), which is similar to the referenced value of 0.512115 ± 7 (Tanaka et al. 2000). For the calculation of $\varepsilon_{Nd}(t)$ values, we have adopted a decay constant for ^{147}Sm of 6.54×10^{-12} $year^{-1}$ (Lugmair and Marti 1978) and chondritic values of $^{143}Nd/^{144}Nd$ (0.512638) and $^{147}Sm/^{144}Nd$ (0.1967) (Jacobsen and Wasserburg 1980). Depleted mantle values of $^{143}Nd/^{144}Nd$ (0.513151), $^{147}Sm/^{144}Nd$ (0.2136) (Jahn and Condie 1995) are using for calculating depleted mantle model ages (T_{DM}).

5 Resules

5.1 Major and trace element geochemistry

The JLY granitic pluton has variable SiO_2 contents from 70.89 wt% to 75.76 wt%, with an average of 72.75 wt%, and has a high alkali ($Na_2O + K_2O$) contents from 7.51 wt% to 8.72 wt% (Table 1). All samples plot in the "subalkalic granite" field (Fig. 3a). Six samples fall in the "alkali-calcic" field and four samples plot in the "calc-alkalic" field (Fig. 3b). They possess intermediate to high Al_2O_3 contents, ranging from 11.44 wt% to 13.20 wt%, with an average of 12.62 wt%. As shown in the plot of A/NK–A/CNK diagram (Fig. 3c), the samples are metaluminous to weakly peraluminous (0.96–1.12). The granite has relatively high $Fe_2O_3^T$ content (2.50 wt%–4.21 wt%) and low MgO (0.23 wt%–0.50 wt%). The $Fe_2O_3^T$/MgO ratios (7.08–10.87, an average of 9.14) are much higher than those of typical S-type granites (average 2.38 of 578 samples), M-type (average 2.37 of 17 samples) and I-type (average 2.27 of 991 samples) (Whalen et al. 1987).

The trace element concentrations of the JLY granite is shown in Table 1. All of the analyzed samples are enriched in rare earth element contents (ΣREE) between 295.1 and 694.3 ppm. In the chondrite-normalized REE patterns (Fig. 4a), the JLY granite has steep, right-inclined, chondrite-normalized patterns with well-developed, negative Eu anomalies (Eu/Eu* = 0.21–0.40). They is also characterized by high contents of high field strength elements (HFSEs) in the primitive mantle-normalized trace element spider diagram (Fig. 4b), such as Zr (289–520 ppm), Y (36.2–68.2 ppm) and Ga (18.4–23.5 ppm). And all the samples show the characteristic negative anomalies in Ba, Sr, Eu, and Ti, and positive anomalies of Th, La, Nd, and Ce, consistent with the pattern of A-type granites (Collins et al. 1982; Whalen et al. 1987). All of the JLY granites plot in the within-plate granite field (Fig. 5a, b), indicating that the granite was formed by intraplate magmatism (Pearce et al. 1984).

5.2 Zircon U–Pb ages and Hf isotopic compositions

The zircons U–Pb isotope analytical results from the JLY granite are listed in Table 2 and the Hf isotopic compositions are presented in Table 3.

The zircon grains are yellow, euhedral, stubby tetragonal prism shapes, with the size of 40–120 μm. In CL images, the zircons show well-developed oscillatory zoning (Fig. 6). Th concentrations vary from 143 to 1719 ppm, and U range from 150 to 3385 ppm, with Th/U ratios from 0.33 to 1.10 (Table 2). All of these indicate that these zircons are of magmatic origin (Hanchar and Rudnick 1995; Rubatto and Williams 2000; Möller et al. 2003; Hoskin and Schaltegger 2003). Twenty spots are selected from domains of homogenous composition and clear oscillatory zoning for U–Pb analysis. Nineteen spot analyses gave similar $^{206}Pb/^{238}U$ ages, with a weighted average age of 224.1 ± 3.3 Ma (Fig. 7).

The zircons that had been done U–Pb dating were selected for Lu–Hf isotope analyses. Fifteen spots yield $^{176}Hf/^{177}Hf$ values of 0.282432–0.282544, and the calculated $\varepsilon_{Hf}(t)$ values ranged from −3.2 to −7.2 (an average of −4.8, Fig. 8a). The two-stage Hf isotopic model ages (T_{2DM}) vary from 1308 to 1525 Ma (an average of 1393 Ma, Fig. 8b).

5.3 Whole-rock Sr–Nd isotopes

Whole rock Sr–Nd isotopic data of the JLY granite are presented in Table 4. Initial $^{87}Sr/^{86}Sr$ and $\varepsilon_{Nd}(t)$ values have been calculated based on the determined zircon U–Pb age of 224 Ma. Medium $(^{87}Sr/^{86}Sr)_i$ ratios (0.705873–0.712647) and negative $\varepsilon_{Nd}(t)$ values (−9.5 to −9.1) have been obtained. The depleted mantle Nd model ages (T_{DM}) of the JLY granite vary from 1606 to 1985 Ma.

6 Discussion

6.1 Evidences for A-type granite

The JLY granite has high alkali contents ($Na_2O + K_2O$ = 7.51 wt%–8.72 wt%), high HFSE contents (Zr + Nb + Ce + Y = 492–868 ppm), high total REE contents

Table 1 Major element (in wt%) and trace element (in ppm) concentrations of the Jinlongyan granite

Sample no.	JLY1	JLY2	JLY3	JLY4	JLY5	JLY6	JLY7	JLY8	JLY9	JLY10
SiO_2	71.34	72.76	75.76	72.29	75.31	73.48	71.33	72.50	71.86	70.89
Al_2O_3	12.98	12.79	11.44	12.93	11.90	12.70	13.02	12.32	13.20	12.94
TiO_2	0.46	0.27	0.23	0.35	0.25	0.32	0.31	0.43	0.45	0.48
$Fe_2O_3^T$	3.54	2.86	2.50	3.28	2.65	3.07	3.10	3.68	3.92	4.21
MnO	0.06	0.06	0.05	0.05	0.05	0.06	0.06	0.07	0.07	0.08
MgO	0.50	0.30	0.23	0.33	0.27	0.32	0.37	0.44	0.44	0.47
CaO	0.99	1.10	1.02	0.86	0.69	1.15	1.49	1.30	0.94	0.90
Na_2O	2.53	2.92	2.98	3.22	2.15	2.55	2.94	2.53	3.28	3.15
K_2O	6.19	5.71	4.53	5.22	5.42	5.78	5.60	5.41	5.06	4.89
P_2O_5	0.12	0.06	0.04	0.07	0.05	0.08	0.07	0.10	0.11	0.10
LOI	0.46	1.09	0.98	0.72	0.68	0.83	1.24	0.90	0.56	0.66
Total	99.17	99.92	99.76	99.32	99.42	100.34	99.53	99.68	99.89	98.77
A/CNK	1.03	0.99	0.98	1.03	1.12	1.01	0.96	1.00	1.05	1.07
$Na_2O + K_2O$	8.72	8.63	7.51	8.44	7.57	8.33	8.54	7.94	8.34	8.04
$Fe_2O_3^T/MgO$	7.08	9.53	10.87	9.94	9.81	9.59	8.38	8.36	8.91	8.96
V	22	7	11	14	8	13	11	17	12	13
Cr	280	260	280	270	310	350	250	220	160	190
Ga	19.3	18.4	19.5	22.4	18.8	18.9	22.0	21.3	21.2	23.5
Rb	270	234	233	233	274	297	300	301	267	296
Sr	134.5	68.0	69.6	96.3	51.0	64.7	90.2	72.3	79.8	79.8
Y	46.6	36.2	40.5	62.4	39.7	53.8	54.0	68.2	53.3	58.2
Zr	446	329	310	446	289	419	407	479	442	520
Nb	27.9	23.0	29.1	40.2	25.3	33.3	36.2	45.5	42.4	48.4
Sn	4	6	8	6	6	6	6	9	8	9
Ba	768	424	268	432	336	394	392	421	293	362
Cs	6.89	2.73	3.87	2.72	5.01	5.73	6.52	6.51	6.68	7.25
Hf	12.3	10.1	10.1	12.9	9.3	12.9	12.0	14.3	13.3	15.0
Ta	1.9	2.5	2.7	3.1	3.0	2.9	2.7	4.3	2.4	3.0
W	2	1	11	2	2	2	3	3	3	2
Th	47.7	39.6	58.7	65.7	44.8	49.3	46.8	50.0	68.2	69.3
U	6.90	7.32	9.72	9.50	9.76	10.90	11.75	10.05	10.25	11.15
La	114.5	74.5	66.7	170.5	72.5	82.4	76.6	88.3	112.0	101.0
Ce	212.0	140.5	132.0	320.0	138.5	158.0	149.0	174.5	207.0	191.0
Pr	22.30	15.40	14.40	34.60	15.20	17.90	16.85	19.85	23.70	21.80
Nd	67.6	47.4	46.0	107.5	48.5	56.2	53.8	65.3	76.3	69.6
Sm	11.10	8.98	9.43	19.30	9.61	11.70	11.90	14.15	15.70	14.55
Eu	1.25	0.82	0.63	1.16	0.66	0.81	0.88	0.97	0.96	0.96
Gd	7.34	6.39	7.02	12.95	7.03	8.53	9.31	11.45	10.70	10.95
Tb	1.13	1.02	1.16	2.04	1.12	1.43	1.50	1.83	1.70	1.74
Dy	6.41	5.68	6.67	10.70	6.21	8.26	8.73	10.60	9.21	9.49
Ho	1.32	1.13	1.31	2.08	1.27	1.71	1.74	2.20	1.88	1.86
Er	3.97	3.20	4.03	5.79	3.80	4.93	5.09	6.44	5.10	5.48
Tm	0.61	0.54	0.69	0.94	0.65	0.84	0.82	1.16	0.79	0.86
Yb	4.12	3.53	4.43	5.86	4.09	5.42	5.24	6.78	4.81	5.41
Lu	0.66	0.57	0.67	0.84	0.60	0.79	0.77	0.96	0.68	0.79
$\sum$REE	454.3	309.7	295.1	694.3	309.7	358.9	342.2	404.5	470.5	435.5
$(La/Yb)_N$	18.74	14.23	10.15	19.62	11.95	10.25	9.86	8.78	15.70	12.59
$(La/Sm)_N$	6.49	5.22	4.45	5.56	4.75	4.43	4.05	3.93	4.49	4.37

Table 1 continued

Sample no.	JLY1	JLY2	JLY3	JLY4	JLY5	JLY6	JLY7	JLY8	JLY9	JLY10
$(Gd/Yb)_N$	1.44	1.46	1.28	1.78	1.39	1.27	1.43	1.36	1.80	1.63
Eu/Eu*	0.40	0.32	0.23	0.21	0.23	0.24	0.25	0.23	0.21	0.22
10,000 Ga/Al	2.81	2.72	3.22	3.27	2.99	2.81	3.19	3.27	3.04	3.43
Zr + Nb + Ce + Y	732.5	528.7	511.6	868.6	492.5	664.1	646.2	767.2	744.7	817.6
T_{Zr} (°C)	881	848	847	884	854	876	863	887	883	903

$A = Al_2O_3$, $C = CaO$, $N = Na_2O$, $K = K_2O$ (all in molar proportion)

$Eu/Eu^* = 2 \times Eu_N/(Sm_N + Gd_N)$

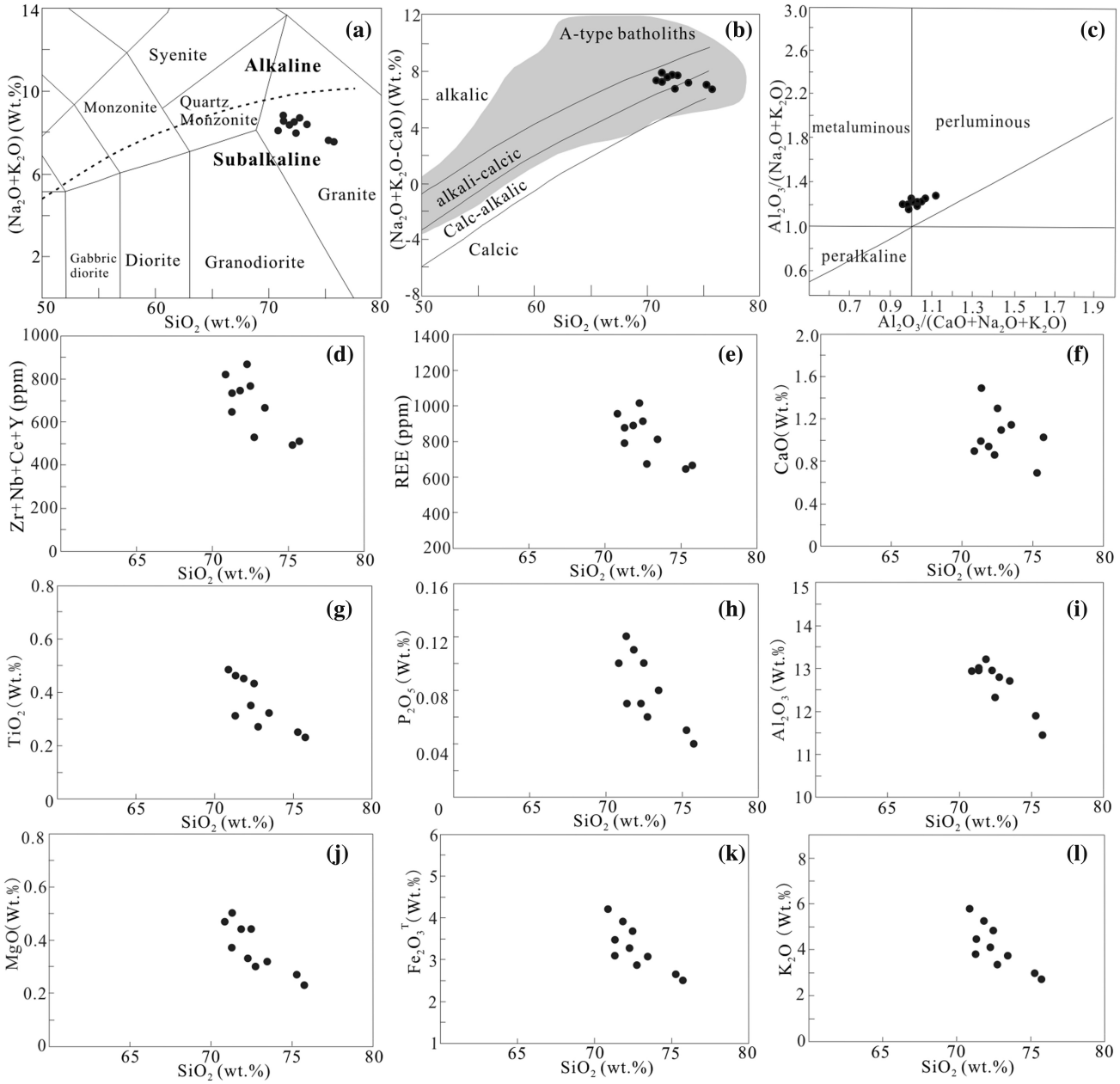

Fig. 3 Chemical classification diagrams for the Jinlongyan granite: **a** total alkalis ($K_2O + Na_2O$) versus SiO_2 diagram (compositional fields from Middlemost 1994); **b** ($Na_2O + K_2O - CaO$) versus SiO_2 diagram (Frost et al. 2001); **c** A/NK versus A/CNK diagram (Maniar and Piccoli 1989); **d–l** Harker plots for the Jinlongyan granite

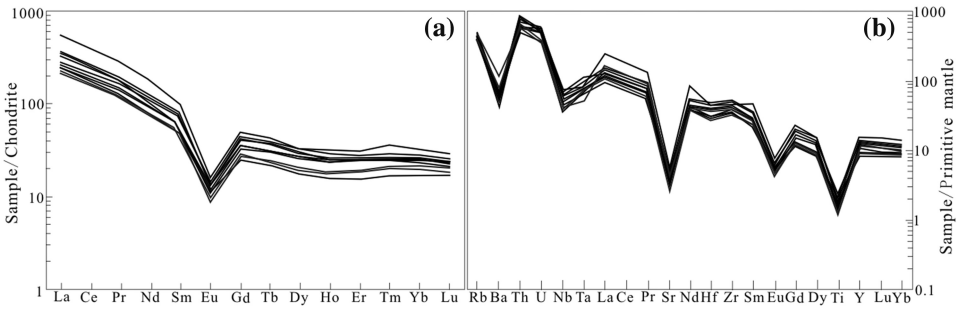

Fig. 4 **a** Chondrite-normalized REE patterns (normalized values are from Boynton 1984) and **b** primitive mantle-normalized trace element patterns (normalized values are from McDonough and Sun 1995) for the Jinlongyan granite

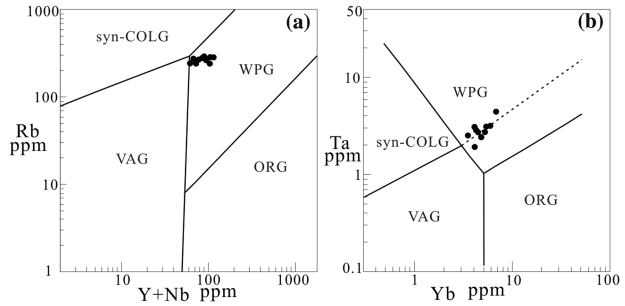

Fig. 5 Trace element diagrams for tectonic discrimination (after Pearce et al. 1984): **a** Rb versus (Y + Nb); **b** Ta versus Yb. *VAG* volcanic-arc granites, *syn-COLG* syn-collisional granites, *WPG* within-plate granites, *ORG* ocean-ridge granites

(295–694 ppm) and high $Fe_2O_3^T$/MgO ratios (7.08–10.87), as well as shows extreme depletion in Ba, Sr, Ti and Eu. These geochemical characteristics are similar to those of A-type granites (Whalen et al. 1987). All of the samples from the JLY granite plot in the A-type granite field in the various chemical classification diagrams of ($K_2O + Na_2O$) versus 10,000 Ga/Al, Nb versus 10,000 Ga/Al, ($K_2O + Na_2O$)/CaO versus (Zr + Nb + Ce + Y), $Fe_2O_3^T$/MgO versus (Zr + Nb + Ce + Y) (Fig. 9a–d) (Whalen et al. 1987). Therefore, they can be classified as A-type granites. According to the geochemical subdivision of A-type granites by Eby (1992), the JLY A-type granite corresponds to the A_2-type granite (Fig. 9e, f).

Table 2 U–Pb dating results of zircons from Jinlongyan granite (determined by LA–ICP–MS)

Spots	Th (ppm)	U (ppm)	Th/U	$^{207}Pb/^{206}Pb$	1σ	$^{207}Pb/^{235}U$	1σ	$^{206}Pb/^{238}U$	1σ	$^{207}Pb/^{235}U$(Ma)	1σ (Ma)	$^{206}Pb/^{238}U$(Ma)	1σ (Ma)
JLY1.1	412	678	0.61	0.05201	0.00249	0.24607	0.01203	0.03431	0.00045	223	10	217	3
JLY1.2	616	1227	0.50	0.05478	0.00218	0.25677	0.00992	0.03413	0.00042	232	8	216	3
JLY1.3	165	150	1.10	0.05689	0.00663	0.26476	0.02962	0.03561	0.00091	238	24	226	6
JLY1.4	143	223	0.64	0.05905	0.00579	0.26586	0.02330	0.03380	0.00075	239	19	214	5
JLY1.5	1030	2559	0.40	0.05225	0.00151	0.24466	0.00705	0.03386	0.00032	222	6	215	2
JLY1.6	265	257	1.03	0.05356	0.00495	0.26208	0.02282	0.03571	0.00071	236	18	226	4
JLY1.7	258	285	0.90	0.05525	0.00333	0.25720	0.01438	0.03420	0.00053	232	12	217	3
JLY1.8	544	1634	0.33	0.05277	0.00250	0.25308	0.01175	0.03469	0.00039	229	10	220	2
JLY1.9	204	303	0.67	0.05236	0.00399	0.25860	0.01811	0.03634	0.00058	234	15	230	4
JLY1.10	307	280	1.09	0.05523	0.00377	0.26458	0.01678	0.03571	0.00057	238	13	226	4
JLY1.11	144	209	0.69	0.06444	0.00484	0.31956	0.02426	0.03659	0.00068	282	19	232	4
JLY1.12	930	1877	0.50	0.05115	0.00162	0.25766	0.00804	0.03650	0.00037	233	6	231	2
JLY1.13	318	399	0.80	0.05438	0.00333	0.26239	0.01594	0.03521	0.00049	237	13	223	3
JLY1.14	363	777	0.47	0.05421	0.00248	0.26211	0.01171	0.03537	0.00042	236	9	224	3
JLY1.15	524	490	1.07	0.05475	0.00327	0.26359	0.01467	0.03528	0.00049	238	12	224	3
JLY1.16	1719	3385	0.51	0.04974	0.00138	0.25965	0.00731	0.03768	0.00041	234	6	238	3
JLY1.17	477	486	0.98	0.05408	0.00391	0.26178	0.01842	0.03594	0.00054	236	15	228	3
JLY1.18	360	535	0.67	0.05163	0.00278	0.25612	0.01454	0.03610	0.00052	232	12	229	3
JLY1.19	287	349	0.82	0.05157	0.00357	0.25324	0.01576	0.03608	0.00061	229	13	228	4
JLY1.20	450	575	0.78	0.05174	0.00274	0.26380	0.01451	0.03692	0.00055	238	12	234	3

Table 3 Hf isotopic compositions of zircon grains from Jinlongyan granite determined by LA–MC–ICPMS

Spots	$^{176}Hf/^{177}Hf$	1σ	$^{176}Lu/^{177}Hf$	1σ	$^{176}Yb/^{177}Hf$	Age (Ma)	εHf(t)	1σ	T_{1DM} (Ma)	T_{2DM} (Ma)	$f_{Lu/Hf}$
JLY1.1	0.282492	0.000012	0.000655	0.000046	0.017947	217	−5.2	0.7	1065	1411	−0.98
JLY1.2	0.282475	0.000015	0.000634	0.000024	0.017031	226	−5.6	0.7	1087	1439	−0.98
JLY1.3	0.282539	0.000018	0.000867	0.000021	0.023407	214	−3.7	0.8	1005	1321	−0.97
JLY1.4	0.282511	0.000018	0.000709	0.000026	0.018993	226	−4.4	0.8	1040	1370	−0.98
JLY1.5	0.282528	0.000017	0.000915	0.000026	0.024803	230	−3.7	0.8	1022	1337	−0.97
JLY1.6	0.282491	0.000015	0.000704	0.000021	0.018741	224	−5.1	0.7	1068	1411	−0.98
JLY1.7	0.282432	0.000014	0.000632	0.000019	0.016809	226	−7.2	0.7	1148	1525	−0.98
JLY1.8	0.282463	0.000016	0.000573	0.000009	0.015383	231	−5.9	0.8	1103	1461	−0.98
JLY1.9	0.282485	0.000016	0.000608	0.000006	0.016140	224	−5.3	0.8	1073	1421	−0.98
JLY1.10	0.282522	0.000013	0.000892	0.000030	0.024137	223	−4.1	0.7	1030	1352	−0.97
JLY1.11	0.282511	0.000015	0.001415	0.000047	0.038544	224	−4.5	0.7	1059	1376	−0.96
JLY1.12	0.282512	0.000013	0.001167	0.000053	0.031757	238	−4.2	0.7	1051	1367	−0.96
JLY1.13	0.282544	0.000018	0.001053	0.000021	0.028613	229	−3.2	0.8	1003	1308	−0.97
JLY1.14	0.282479	0.000021	0.000825	0.000008	0.022851	228	−5.5	0.9	1087	1432	−0.98
JLY1.15	0.282516	0.000015	0.001046	0.000011	0.027762	234	−4.1	0.7	1043	1361	−0.97

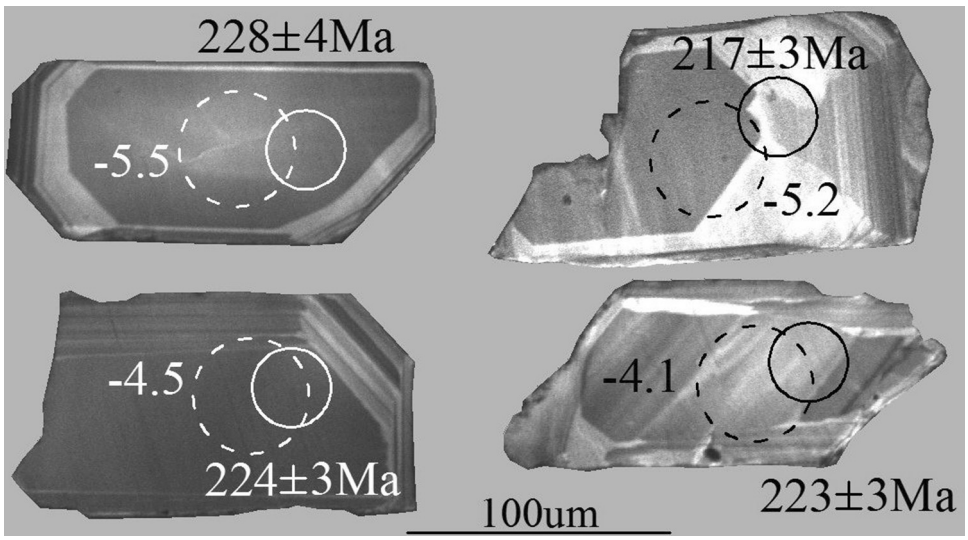

Fig. 6 Representative cathodoluminescence (CL) images, showing the laser analytic spots, $^{206}Pb/^{238}U$ ages and $\varepsilon_{Hf}(t)$ values of zircons from the Jinlongyan granite. *Solid circles* show the locations of U–Pb age analyses, and *dotted circles* show the locations of Hf isotope analyses

A-type granites are generally considered to be derived from relatively anhydrous and high-temperature magmas (Loiselle and Wones 1979; Bonin 2007). Zircon saturation thermometry (T_{Zr}) provides a simple and robust means to estimate the magma temperature of granites (Watson and Harrison 1983). T_{Zr} calculated from bulk rock compositions provide minimum estimates of magma temperature if the magma was undersaturated in Zr, but maxima if it was saturated (Miller et al. 2003). The JLY granite is absent from restitic and inherited zircons indicating that it was likely undersaturated in Zr. Thus, the calculated T_{Zr} of the JLY granite (847–903 °C) is likely to be a minimum estimate of its initial magma temperature (Table 1). This calculated T_{Zr} is similar to those for many other A-type granites (Sun et al. 2011; Li et al. 2012; Zhao et al. 2013), but higher than those of common I- and S-type granites (usually lower than 800 °C, King et al. 1997; Jiang et al. 2009). The relatively high melting or magma temperatures of the JLY granite suggest that they were derived from a refractory or dry source.

As shown by the Harker diagrams (Fig. 3d–l), the major oxides show linear trends for the JLY granite, indicating that fractional crystallization plays a dominant role in the evolution of the JLY granite. The samples are

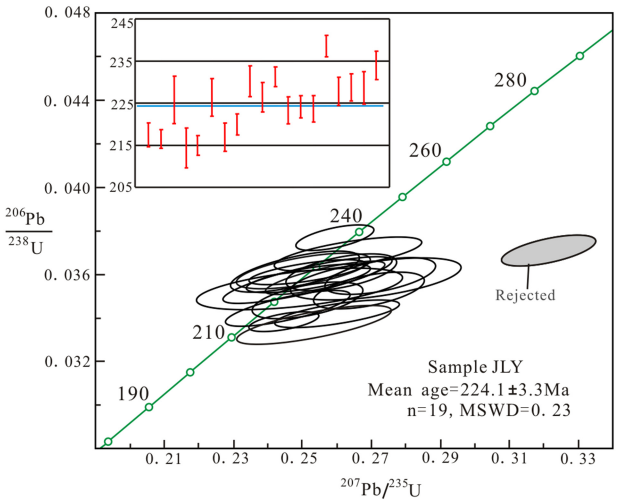

Fig. 7 U–Pb concordia diagram of zircon from the Jinlongyan granite

characterized by low MgO contents, which are interpreted to be due to the fractionation of MgO-rich minerals such as hornblende. A negative TiO_2 anomaly is commonly related to ilmenite or titanite fractionation. In addition, P_2O_5 contents decrease with increasing SiO_2, showing apatite fractionation. It is known that CaO is mainly concentrated in plagioclase and apatite; $Fe_2O_3^T$ in magnetite. Therefore, the decrease in CaO and $Fe_2O_3^T$ with increasing SiO_2 demonstrates that the JLY granite was possibly produced by fractional crystallization of plagioclase and magnetite. The negative correlation of K_2O and Al_2O_3 with SiO_2 indicates that K-feldspar in the residual magma had decreased with the fractional crystallization of other minerals. Chondrite-normalized REE patterns and primitive mantle-normalized trace element patterns (Fig. 4a, b) also support this opinion that magmas were fractionated to some degree during their evolution. From the REE patterns, hornblende may be considered to be an important phase fractionated from magmas because it is able to produce a fairly flat-HREE pattern without significant HREE fractionation in intermediate and acidic magmas (Martin et al. 1994; Han et al. 1997). The presence of Eu, Sr and Ba negative anomalies in the JLY granite is due to fractionation of both plagioclase and K-feldspar.

6.2 Petrogenesis of the A-type JLY granite

The origin of A-type granites is still under debates, mainly because so many compositional variations have been found, and there is no consensus on the origin of A-type granites (Bonin 2007). Several petrogenetic models have

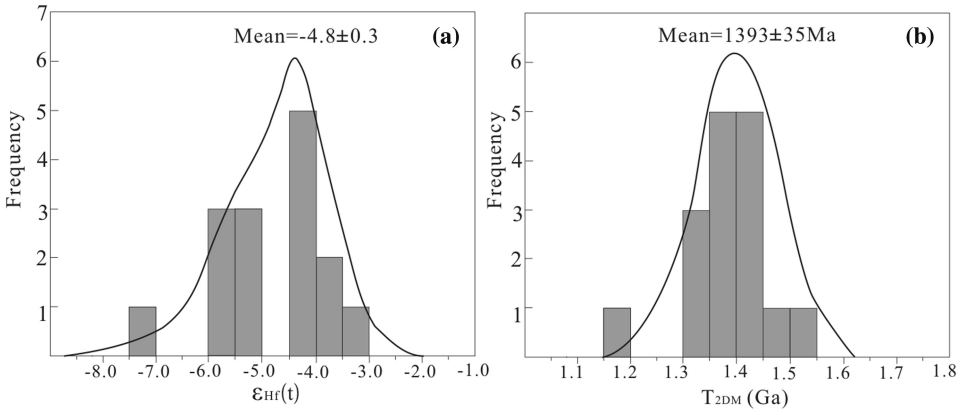

Fig. 8 **a** Histograms of zircon $\varepsilon_{Hf}(t)$ values; **b** two-stage Hf model ages (T_{2DM}) from the Jinlongyan granite

Table 4 Sr–Nd isotopic compositions of the Jinlongyan granite

Sample	Age (Ma)	$^{87}Rb/^{86}Sr$	$^{87}Sr/^{86}Sr$	Error(2SE)	$(^{87}Sr/^{86}Sr)i$	$^{147}Sm/^{144}Nd$	$^{143}Nd/^{144}Nd$	Error(2SE)	$\varepsilon_{Nd}(t)$	$f_{Sm/Nd}$	T_{DM} (Ma)
JLY2	224	9.9473	0.741341	0.000007	0.709650	0.1148	0.512030	0.000004	−9.5	−0.42	1726
JLY4	224	6.9940	0.734929	0.000008	0.712647	0.1088	0.512045	0.000003	−9.1	−0.45	1606
JLY6	224	13.2693	0.748147	0.000006	0.705873	0.1262	0.512058	0.000006	−9.3	−0.36	1900
JLY8	224	12.0344	0.745595	0.000006	0.707255	0.1313	0.512076	0.000004	−9.1	−0.33	1985
JLY9	224	9.6718	0.739687	0.000009	0.708874	0.1247	0.512053	0.000005	−9.4	−0.37	1878

$f_{Sm/Nd} = (^{147}Sm/^{144}Nd)_s/(^{147}Sm/^{144}Nd)_{CHUR} - 1$

$\varepsilon_{Nd}(t) = \{[(^{143}Nd/^{144}Nd)_s - (^{147}Sm/^{144}Nd)_s \times (e^{\lambda t} - 1)]/[(^{143}Nd/^{144}Nd)_{CHUR,0} - (^{147}Sm/^{144}Nd)_{CHUR,0} \times (e^{\lambda t} - 1)] - 1\} \times 10000$

$T_{DM} = 1/\lambda \times \ln\{1 + [(^{143}Nd/^{144}Nd)s - (^{143}Nd/^{144}Nd)_{DM}]/[(^{147}Sm/^{144}Nd)_s - (^{147}Sm/^{144}Nd)_{DM}]\}$

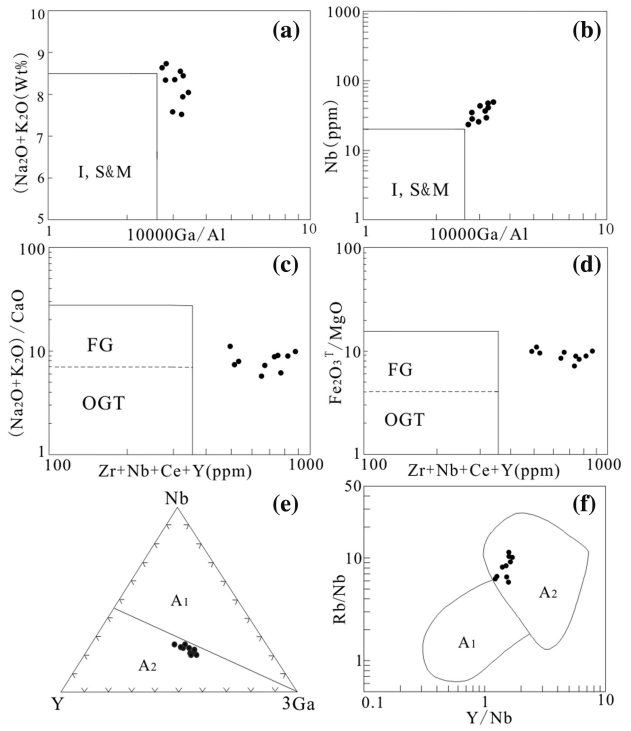

Fig. 9 Chemical classification diagrams: **a** ($K_2O + Na_2O$) versus 10000 Ga/Al; **b** Nb versus 10,000 Ga/Al; **c** ($K_2O + Na_2O$)/CaO versus (Zr + Nb + Ce + Y); **d** $Fe_2O_3^T$/MgO versus (Zr + Nb + Ce + Y) (Whalen et al. 1987); **e** Nb–Y–Ga triangle diagram; **f** Rb/Nb versus Y/Nb (after Eby 1992); *FG* fractionated felsic granites, *OGT* unfractionated M-, I- and S-type granites

been proposed for the origin of A-type granites, including: (1) direct fractionation products of mantle-derived alkaline basalts (Turner et al. 1992; Litvinovsky et al. 2002; Mushkin et al. 2003); (2) low degrees of partial melting of lower-crustal granulites that were depleted in incompatible elements by previous melt extraction (Collins et al. 1982; Clemens et al. 1986; Whalen et al. 1987; King et al. 1997); (3) anatexis of undeplated I-type tonalitic crustal sources (Sylvester 1989; Creaser et al. 1991; Skjerlie and Johnston 1992; Patino-Douce 1997); (4) hybridization between anatectic granitic and mantle-derived mafic magmas(Kerr and Fryer 1993; Wickham et al. 1996; Yang et al. 2006; Zhao et al. 2012). However, among these petrogenetic models, interaction of mantle-derived magma with crustal rocks, and melting of deep continental crust are considered as the most important mechanism (Rämö and Haapala 1995; Bonin 1996).

The negative $\varepsilon_{Hf}(t)$ values (−7.2 to −3.2), $\varepsilon_{Nd}(t)$ values (−9.5 to −9.1), medium $(^{87}Sr/^{86}Sr)_i$ ratios (0.705873–0.712647) and relatively low MgO content (0.23 wt% –0.50 wt%) of the JLY A-type granite rule out the possibility of direct crystallization differentiation from mantle-derived magma. In addition, large volumes of mafic-intermediate rocks, as would be expected if extensive fractional crystallization took place, are usually absent in the area where A-type granites occur. Moreover, basic to intermediate microgranular enclave, which is often indicative of mantle-derive magma mingled in granitic magma (Chappell 1996; Janousek et al. 2004), cannot be found in the JLY pluton. Thus, we argue that the JLY A-type granite was not likely formed through mixing or mingling of the mantle- and crustal-derived magmas. Some highly fractionated felsic granites have geochemical characteristics which overlap those for typical A-type granites (Whalen et al. 1987). Figure 9c, d show that Jinlongyan rocks plot in the A-type field. Yet, they are also highly fractionated rocks, but not from I-, or S-type granites. It is possible that the parental magma of the JLY A-type granitic pluton was generated from old crustal rocks, which is also supported by the following evidences: (1) On the $\varepsilon_{Nd}(t)$ versus age diagram, all the samples plot in the field of Nd evolution of the proterozoic crust in the SCB (Fig. 10); (2) As discussed above, the JLY A-type granite corresponds to the A_2-type granite (Fig. 9e, f). Eby (1992) subdivided A-type granite into two sub-types (A_1 and A_2) and suggested that the A_2-type granite was derived from the partial melting of continental crustal or underplated crust.

According to the discussion above, the calculated T_{Zr} of the JLY granite is between 847 and 903 °C, which is higher than those of common I-type granites (usually lower than 800 °C, King et al. 1997; Jiang et al. 2009). The primary magma for the JLY granite was anhydrous and had a high melting temperature, suggesting that the crustal sources had been dehydrated and/or melt depleted, and were granulitic metavolcanic and/or metasedimentary rocks (Collins et al. 1982). The crustal basement in the Cathaysia Block experienced strongly reworking processes and melt extracting events during the Caledonian Wuyi Orogeny (Zeng et al. 2008; Li et al. 2010), which is conducive to the

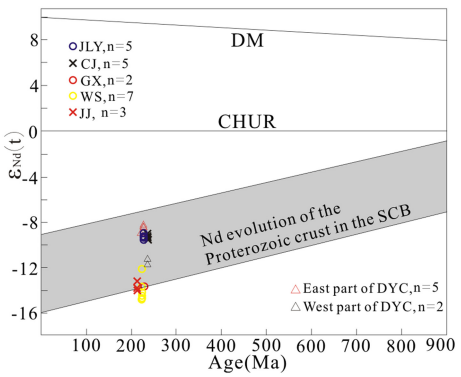

Fig. 10 Age versus $\varepsilon_{Nd}(t)$ values diagram. *DM* depleted mantle, *CHUR* chondritic uniform reservoir. Data of Nd evolution of the Proterozoic crust in the SCB is after Shen et al. (1993)

granulitization of metavolcanic and metasedimentary rocks at this period. Moreover, studies on Nd–Hf isotopic data suggest that the JLY granite has Paleo-Mesoproterozoic T_{DM} ages of Nd and Hf isotopes. Therefore, we suggest that the JLY granitic pluton was derived from partial melting of the Meso-Paleoproterozoic crustal basement rocks which had been granulitized during an earlier thermal event.

6.3 Implication for the tectonic setting

The Indosinian granitic rocks are distributed sporadically within central SCB, and are widespread not only in Fujian Province but also in other regions in the SCB (Fig. 1). Previous studies have shown that more than 90% of the Indosinian granites in South China are S- or I-type granites (Zhou et al. 2006). Mesozoic A-type granites in eastern South China attracted much attention because they have important tectonic implications. A-type granites generally form in extensional tectonic environments regardless of the origin of the magma source (Eby 1992; Turner et al. 1992; Whalen et al. 1987). In the last several decades, the dynamic background of the large-scale tectonic-magmatic activities in Late Paleozoic to Early Mesozoic in Southern China has been controversial (Ren 1964, 1991; Holloway 1982; Hsü et al. 1990; Wang et al. 2005; Li and Li 2007; Lepvrier et al. 2004, 2008; Zhou et al. 2006; Shu et al. 2008).

Our new zircon LA–ICP–MS U–Pb age data on the JLY granite shows late Triassic emplacement ages of 224 Ma (Fig. 7). Contemporaneous granites have been reported along the southeast margin of the SCB (Fig. 1), including the Wengshan A-type granite (224 Ma) (Sun et al. 2011), the Gaoxi and Caijiang A-type granites (228–229 Ma) (Zhao et al. 2013), Dayinchang A-type granite (224–237 Ma) (Wang et al. 2013a), Xiaotao aluminous A-type granites (222 Ma) (Wang et al. 2007a), as well as other intrusive suites that are exposed mainly in the central SCB (202–248 Ma) (Wang et al. 2013b). The distribution of these A-type granitic plutons distributed in the SCB are parallel to the NE-trending faults (Fig. 1). It is indicated that major NE-trending strike-slip faults might have played an important role in the emplacement of the A-type granitic plutons. Given that all of these A-type granites were emplaced at a similar time, it is possible that the JLY A-type granite are part of a more extensive A-type magmatic suite within the southeastern margin of the SCB.

Superimposed folding (Zhang et al. 2009), ductile deformation (Faure 1996; Lin et al. 2000; Chu et al. 2012a, b) and metamorphism (Wang et al. 2012; Xiang et al. 2008; Yu et al. 2009, 2012) indicate that the SCB should be under compressional tectonic regime in the Triassic due to collisional orogeny around the southern margin of the SCB (Yu et al. 2007). Continent–continent collision of the Northern Indosinian block with the SCB occurred from 258 to 242 Ma along the Song-Ma belt (Carter et al. 2001; Lepvrier et al. 2004). The peak metamorphism associated with collision between the North China and SCB was dated at 240–225 Ma along the Dabie-Sulu ultrahigh-pressure metamorphic belt (Li et al. 1993; Zheng 2008). Thus, Indosinian granites in the SCB formed almost simultaneously between the collision of North China Block with the SCB and the collision of the Indosinian block with the SCB. These two collision belts resulted in a significant compressional stress on the SCB which was clamped. Although the overall tectonic regime of the SCB at the late Permian–middle Triassic was compressional, the A-type granites that are indicative of extension in the southeastern coast appeared in the local areas of the Zhejiang, Fujian, and Jiangxi provinces (Fig. 1).

Based on previous studies and this work, the following suggestion is put forward: EW-trending strike-slip faults and NE-trending local extensional faults developed during the collision between the SCB and the Indochina Block or the North China Block (Wang et al. 2013b); The local NE-trending extensional faults caused by the above one or two collisions were conducive to the forming of A-type granites including JLY, Wengshan, Gaoxi, Caijiang, Dayinchang and Xiaotao A-type granites. Therefore, the tectonic environment of the SCB probably transformed from collision into the within-plate post-collisional setting since about 224 Ma.

7 Conclusions

Zircon U–Pb dating yields precise crystallization ages of 224 Ma for the JLY granite in Fujian Province, South China. Petrologic, geochemical and isotopic data demonstrate that the JLY granite belong to A-type granite, and reveal that the parental magma of JLY granite was derived from partial melting of Meso-Paleoproterozoic crustal rocks that had been granulitized during an earlier thermal event. Our study of the JLY A-type granite, together with other Triassic A-type granites in South China, defines an extensional environment in the late Triassic which probably was caused by the collision of the SCB with Indochina Block or North China Block. .

Acknowledgements We thank Huadong Gong for his help in the determination of zircon U–Pb age using LA–ICPMS, Lei Xu for her help during zircon Hf isotopic analyses by LA–MC–ICPMS, and Wei Pu for his help in Sr–Nd isotopic analyses. We are also grateful to the guest editors and the reviewer Tynie Alfante for constructive suggestions and criticisms in reviewing the manuscript. The work was

financially supported by the Chinese National Natural Science Foundation (41373024) and Opening Foundation of State Key Laboratory of Ore Deposit Geochemistry, Institute of Geochemistry, Chinese Academy of Sciences (201307).

References

Andersen T (2002) Correction of common lead in U–Pb analyses that do not report 204Pb. Chem Geol 192:59–79

Blichert-Toft J, Albarède F (1997) The Lu–Hf isotope geochemistry of chondrites and the evolution of the mantle-crust system. Earth Planet Sci Lett 148:243–258

Bonin B (1996) A-type granite ring complexes: mantle origin through crustal filters and the anorthosite-rapakivi magmatism connection. In: Demaiffe D (ed) Petrology and geochemistry of magmatic suites of rocks in the continental and oceanic crusts. A volume dedicated to Professor Jean Michot. ULB-MRAC, Bruxelles, pp 201–218

Bonin B (2007) A-type granites and related rocks: evolution of a concept, problems and prospects. Lithos 97(1–2):1–29

Boynton WV (1984) Geochemistry of the rare earth elements: meteorite studies. In: Henderson (ed) Rare Earth element geochemistry. Elsevier, New York, pp 63–114

Carter A, Roques D, Bristow C, Kinny P (2001) Understanding Mesozoic accretion in Southeast Asia: significance of Triassic thermotectonism (Indosinian orogeny) in Vietnam. Geology 29(3):211–214

Chappell BW (1996) Magma mixing and the production of compositional variation within granite suites: evidence from the granites of southeastern Australia. J Petrol 37:449–470

Chen A (1999) Mirror-image thrusting in the South China Orogenic Belt: tectonic evidence from western Fujian, southeastern China. Tectonophysics 305:497–519

Chen JF, Jahn BM (1998) Crustal evolution of southeastern China: Nd and Sr isotopic evidence. Tectonophysics 284:101–133

Chen HH, Sun X, Li JL, Haag M, Dobson J, Hsu JH, Heller F (1994) Paleomagnetic constraints on early Triassic tectonics of South China. Sci Geol Sin 29(1):1–9

Chu Y, Faure M, Lin W, Wang QC, Ji WB (2012a) Tectonics of the Middle Triassic intracontinental Xuefengshan Belt, South China: new insights from structural and chronological constraints on the basal decollement zone. Int J Earth Sci 101(8):2125–2150

Chu Y, Faure M, Lin W, Wang QC (2012b) Early Mesozoic tectonics of the South China block: insights from the Xuefengshan intracontinental orogen. J Asian Earth Sci 61:199–220

Clemens JD, Holloway JR, White AJR (1986) Origin of an A-type granite: experimental constraints. Am Mineral 71:317–324

Collins WJ, Beams SD, White AJR, Chappell BW (1982) Nature and origin of A-type granites with particular reference to southeastern Australia. Contrib Miner Petrol 80:189–200

Creaser RA, Price RC, Wormald RJ (1991) A-type granites revisited: assessment of a residual-source model. Geology 19:163–166

Dai BZ, Jiang SY, Jiang YH, Zhao KD, Liu DY (2008) Geochronology, geochemistry and Hf–Sr–Nd isotopic compositions of Huziyan mafic xenoliths, southern Hunan Province, South China: Petrogenesis and implications for lower crust evolution. Lithos 102(1):65–87

Eby GN (1992) Chemical subdivision of the A-type granitoids: petrogenetic and tectonic implications. Geology 20:641–644

Faure M (1996) Extensional tectonics within a subduction-type orogen: the case study of the Wugongshan dome (Jiangxi Province, south-eastern China). Tectonophysics 263:77–106

Faure M, Lepvrier C, Nguyen VV, Vu VT, Lin W, Chen ZC (2014) The South China block-Indochina collision: Where, when, and how? J Asian Earth Sci 79:260–274

Frost BR, Barnes CG, Collina WJ, Arculus RJ, Ellis DJ, Frost CD (2001) A geochemical classification for granitic rocks. J Petrol 42:2033–2048

Fujian Bureau of Geology (1985) Regional geology of Fujian Province. Geological Publishing House, Beijing

Gao WL, Wang ZX, Song WJ, Wang DX, Li CL (2014) Zircon U–Pb geochronology, geochemistry and tectonic implications of Triassic A-type granites from southeastern Zhejiang, South China. J Asian Earth Sci 96:255–268

Griffin WL, Wang X, Jackson SE, Pearson NJ, O'Reilly SY, Xu X, Zhou X (2002) Zircon chemistry and magma mixing, SE China: in situ analysis of Hf isotopes, Tonglu and Pingtan igneous complexes. Lithos 61(3–4):237–269

Griffin WL, Pearson NJ, Belousova EA, Saeed A (2006) Comment: Hf-isotope heterogeneity in standard zircon 91500. Chem Geol 233:358–363

Guo F, Fan WM, Lin G, Lin YX (1997) Sm–Nd isotopic age and genesis of gabbro xenolith in Daoxian Countiy, Hunan Province. Chin Sci Bull 42(21):1661–1663

Han BF, Wang SG, Jahn BM, Hong DW, Kagami H, Sun YL (1997) Depleted mantle source for the Ulungur River A-type granites from North Xinjiang, China: geochemistry and Nd–Sr isotopic evidence, and implications for Phanerozoic crustal growth. Chem Geol 138:135–159

Hanchar JM, Rudnick RL (1995) The application of cathodoluminescence and back-scattered electron imaging to dating zircons from lower crustal xenoliths. Lithos 36:289–303

He ZY, Xu XS, Niu Y (2010) Petrogenesis and tectonic significance of aMesozoic granite–syenite–gabbro association from inland South China. Lithos 119(3–4):621–641

Holloway NH (1982) North Palawan Block, Philippines: its relation to Asian mainland and role in evolution of South China Sea. Am Assoc Pet Geol Bull 66:1355–1383

Hoskin PWO, Schaltegger U (2003) The composition of zircon and igneous and metamorphic petrogenesis. Rev Mineral Geochem 53:27–62

Hsieh PS, Chen CH, Yang HJ, Lee CY (2008) Petrogenesis of the Nanling Mountains granites from South China: constraints from systematic apatite geochemistry and whole-rock geochemical and Sr–Nd isotope compositions. J Asian Earth Sci 33:428–451

Hsü KJ, Li JL, Chen HH, Wang QC, Sun S, Sengör AMC (1990) Tectonics of South China: key to understanding west Pacific geology. Tectonophysics 183:9–39

Hu ZC, Liu YS, Gao S, Liu WG, Zhang W, Tong XR, Lin L, Zong KQ, Li M, Chen HH, Zhou L, Yang L (2012) Improved in situ Hf isotope ratio analysis of zircon using newly designed X skimmer cone and Jet sample cone in combination with the addition of nitrogen by laser ablation multiple collector ICP–MS. J Anal At Spectrom 27:1391–1399

Jacobsen SB, Wasserburg GJ (1980) Sm–Nd isotopic evolution of chondrites. Earth Planet Sci Lett 50:139–155

Jahn BM (1974) Mesozoic thermal events in southeast China. Nature 248:480–483

Jahn BM, Condie KC (1995) Evolution of the Kaapvaalcraton as viewed from geochemical and Sr–Nd isotopic analyses of intracratonic pelites. Geochim Cosmochim Acta 59(11):2239–2258

Janousek V, Braithwaite CJR, Bowes DR, Gerdes A (2004) Magma-mixing in the genesis of Hercynian calc-alkaline granitoids: an integrated petrographic and geochemical study of the Sazava intrusion, Central Bohemian Pluton, Czech Republic. Lithos 78:67–99

Jiang YH, Jiang SY, Dai BZ, Liao SY, Zhao KD, Ling HF (2009) Middle to late Jurassic felsic and mafic magmatism in southern Hunan Province, southeast China: implications for a continental arc to rifting. Lithos 107(3–4):185–204

Kerr A, Fryer BJ (1993) Nd isotope evidence for crust-mantle interaction in the generation of A-type granitoid suites in Labrador, Canada. Chem Geol 104(1–4):39–60

King PL, White AJR, Chappell BW, Allen CM (1997) Characterization and origin of aluminous A-type granites from the Lachlan Fold Belt, Southeastern Australia. J Petrol 38(3):371–391

Lepvrier C, Maluski H, Vu VT, Leyreloup A, Thi P, Van VN (2004) The Early Triassic Indosinian Orogeny in Vietnam (Truong Son Belt and Kontum Massif): implications for the geodynamic evolution of Indochina. Tectonophysics 393:87–118

Lepvrier C, Vuong NV, Maluski H, Thi PT, Vu TV (2008) Indosinian tectonics in Vietnam. Comptes Rendus Geosci 340:94–111

Li ZX, Li XH (2007) Formation of the 1300-km-wide intracontinental orogen and postorogenic magmatic province in Mesozoic South China: aflat-slab subduction model. Geology 35(2):179–182

Li SG, Xiao YL, Liou DL, Chen YZ, Ge NJ, Zhang ZQ, Sun SS, Cong BL, Zhang RY, Hart SA, Wang SS (1993) Collision of the North China and Yangtse Blocks and formation of coesite-bearing eclogites: timing and processes. Chem Geol 109:89–111

Li ZX, Li XH, Wartho JA, Clark C, Li WX, Zhang CL, Bao C (2010) Magmatic and metamorphic events during the early Paleozoic Wuyi-Yunkai orogeny, southeastern South China: new age constraints and pressure-temperature conditions. Geol Soc Am Bull 122(5–6):772–793

Li WY, Ma CQ, Liu YY, Robinson PT (2012) Discovery of the Indosinian aluminum A-type granite in Zhejiang Province and its geological significance. Sci China Earth Sci 55:13–25

Liang XQ, Li XH (2005) Late Permian to Middle Triassic sedimentary records in Shiwandashan Basin: implication for the Indosinian Yunkai orogenic Belt, South China. Sed Geol 177:297–320

Lin W, Faure M, Moni EP, Scharer U, Zhang LS, Sun Y (2000) Tectonics of SE China: new insights from the Lushan massif (Jiangxi Province). Tectonics 19(5):852–871

Litvinovsky BA, Jahn BM, Zanvilevich AN, Saunders A, Poulain S, Kuzmin DV, Reichow MK, Titov AV (2002) Petrogenesis of syenite-granite suites from the Bryansky Complex (Transbaikalia, Russia): implications for the origin of A-type granitoid magmas. Chem Geol 189(1–2):105–133

Liu YS, Hu ZC, Gao S, Detlef G, Xu J, Gao CG, Chen HH (2008) In-situ analysis of major and trace elements of anhydrous minerals by LA–ICP–MS without applying an internal standard. Chem Geol 257:34–43

Liu YS, Gao S, Hu ZC, Gao CG, Zong KQ, Wang DB (2010) Continental and oceanic crust recycling-induced melt-peridotite interactions in the Trans-North China Orogen: U–Pb dating, Hf isotopes and trace elements in zircon from mantle xenoliths. J Petrol 51:537–571

Loiselle MC, Wones DR (1979) Characteristics and origin of anorogenic granites. Abstracts of papers to be presented at the Annual Meetings of the Geological Society of America and Associated Societies, San Diego, CA, November 5–8, 11(7):468

Ludwig KR (2003) User's manual for Isoplot/Ex, Version 3.00. A geochronological toolkit for microsoft excel. Berkeley Geochronol Cent Spec Publ 4:1–70

Lugmair GW, Marti K (1978) Lunar initial 143Nd/144Nd: differential evolution of the lunar crust and mantle. Earth Planet Sci Lett 39:349–357

Maniar PD, Piccoli PM (1989) Tectonic discrimination of granitoids. Bull Geol Soc Am 101:635–643

Martin H, Bonin B, Capdevila R, Jahn BM, Lameyre J, Wang Y (1994) The Kuiqi peralkaline granitic complex (SE China): petrology and geochemistry. J Petrol 35:983–1015

McDonough WF, Sun SS (1995) The composition of the Earth. Chem Geol 120(3–4):223–253

Meng QR, Zhang GW (1999) Timing of collision of the North and South China blocks: controversy and reconciliation. Geology 27(2):123–126

Middlemost EAK (1994) Naming materials in the magma/igneous rock system. Earth Sci Rev 37(3–4):215–224

Miller CF, McDowell SM, Mapes RW (2003) Hot and cold granites? Implications of zircon saturation temperatures and preservation of inheritance. Geology 31(6):529–532

Möller A, O'Brien PJ, Kennedy A (2003) Linking growth episodes of zircon and metamorphic textures to zircon chemistry: an example from the ultrahigh-temperature granulites of Rogaland (SW Norway). EMU Notes Mineral 5:65–82

Mushkin A, Navon O, Halicz L, Hartmann G, Stein M (2003) The petrogenesis of A-type magmas from the Amram Massif, Southern Israel. J Petrol 44(5):815–832

Patiño-Douce AE (1997) Generation of metaluminous A-type granites by low-pressure melting of calc-alkaline granitoids. Geology 25:743–746

Pearce JA, Harris NBW, Tindle AG (1984) Trace element discrimination diagrams for the tectonic interpretation of granitic rocks. J Petrol 25:956–983

Pirajno F, Ernst RE, Borisenko AS, Fedoseev G, Naumov EA (2009) Intraplate magmatism in Central Asia and China and associated metallogeny. Ore Geol Rev 35:114–136

Pu W, Zhao KD, Ling HF, Jiang SY (2004) High precision Nd isotope measurement by Triton TI mass spectrometry. Acta Geosci Sin 25:271–274 **(in Chinese with English abstract)**

Pu W, Gao JF, Zhao KD, Ling HF, Jiang SY (2005) Seperation method of Rb–Sr, Sm–Nd using DCTA and HIBA. J Nanjing Univ (Nat Sci) 41:445–450 **(in Chinese with English abstract)**

Rämö OT, Haapala I (1995) One hundred years of rapakivi granite. Mineral Petrol 52:129–185

Ren JS (1964) A preliminary study on pre-Devonian geotectonic problems of southeastern China. Acta Geol Sin 44(4):418–431

Ren JS (1991) On the geotectonics of southern China. Acta Geol Sina (Engl Ed) 4(2):11–136

Rubatto D, Williams IS (2000) Imageing, trace element geochemistry and mineral inclusions: linking U–Pb ages with metamorphic conditions. EOS 21:25

Scherer E, Münker C, Mezger K (2001) Calibration of the lutetium–hafnium clock. Science 293:683–687

Shen WZ, Zhu JC, Liu CS, Xu SJ, Ling HF (1993) Sm–Nd isotopic study of basement metamorphic rocks on south China and its constraint on material sources of granitoids. Acta Petrol Sin 9(2):115–124 **(in Chinese with English abstract)**

Shu LS, Faure M, Wang B, Zhou XM, Song B (2008) Late Palaeozoic-early Mesozoic geological features of South China: response to the Indosinian collision events in Southeast Asia. Comptes Rendus Geosci 340:151–165

Skjerlie KP, Johnston AD (1992) Vapor-absent melting at 10 kbar of a biotite-and amphibole-bearing tonalitic gneiss: implications for the generation of A-type granites. Geology 20:263–266

Sun Y, Ma CQ, Liu YY, She ZB (2011) Geochronological and geochemical constraints on the petrogenesis of late Triassic aluminous A-type granites in southeast China. J Asian Earth Sci 42:1117–1131

Sylvester PJ (1989) Post-collisional alkaline granites. J Geol 97:261–280

Tanaka T, Togashi S, Kamioka H et al (2000) JNdi-1: a neodymium isotopic reference in consistency with LaJolla neodymium. Chem Geol 168(3–4):279–281

Tang LM, Chen HL, Dong CW, Yang SF, Shen ZY, Cheng XG, Fu LL (2013) Middle triassic post-orogenic extension on hainan island: chronology and geochemistry constraints of bimodal intrusive rocks. Sci China Earth Sci 56(5):783–793

Turner SP, Foden JD, Morrison RS (1992) Derivation of some A-type magmas by fractionation of basaltic magma: an example from the Padthaway Ridge, South Australia. Lithos 28(2):151–179

Wan Y, Liu D, Xu M, Zhuang J, Song B, Shi Y, Du L (2007) SHRIMP U–Pb zircon geochronology and geochemistry of metavolcanic and metasedimentary rocks in northwestern Fujian, Cathaysia block, China: tectonic implications and the need to redefine lithostratigraphic units. Gondwana Res 12(1–2):166–183

Wang J, Li ZX (2003) History of Neoproterozoic rift basins in South China: implications for Rodinia break-up. Precambr Res 122:141–158

Wang Q, Li JW, Jian P, Zhao ZH, Xiong XL, Bao ZW, Xu JF, Li CF, Ma JL (2005) Alkaline syenites in eastern Cathaysia (South China): link to Permian–Triassic transtension. Earth Planet Sci Lett 230:339–354

Wang LJ, Yu JH, Xu XS, Xie L, Qiu JS, Sun T (2007a) Formation age and origin of the Gutian-Xiaotao granitic complex in the southwestern Fujian province, China. Acta Petrol Sin 23(6):1470–1484 **(in Chinese with English abstract)**

Wang YJ, Fan WM, Sun M, Liang XQ, Zhang YH, Peng TP (2007b) Geochronological, geochemical and geothermal constraints on petrogenesis of the Indosinian peraluminous granites in the South China Block: a case study in the Hunan Province. Lithos 96:475–502

Wang YJ, Wu CM, Zhang AM, Fan WM, Zhang YH, Zhang YZ, Peng TP, Yin CQ (2012) Kwangsian and Indosinian reworking of the eastern South China Block: constraints on zircon U–Pb geochronology and metamorphism of amphibolites and granulites. Lithos 150:227–242

Wang KX, Sun T, Chen PR, Ling HF, Xiang TF (2013a) The geochronological and geochemical constraints on the petrogenesis of the Early Mesozoic A-type granite and diabase in northwestern Fujian province. Lithos 179:364–381

Wang YJ, Fan WM, Zhang GW, Zhang YH (2013b) Phanerozoic tectonics of the South China Block: key observations and controversies. Gondwana Res 23(4):1273–1305

Watson EB, Harrison TM (1983) Zircon saturation revisited: temperature and composition effects in a variety of crustal magma types. Earth Planet Sci Lett 64:295–304

Whalen JB, Currie KL, Chappell BW (1987) A-type granites: geochemical characteristics, discrimination and petrogenesis. Contrib Miner Petrol 95(4):407–419

Wickham SM, Alberts AD, Zanvilevich AN, Litvinovsky BA, Bindeman IN, Schauble EA (1996) A stable isotope study of anorogenic magmatism in East Central Asia. J Petrol 37(5):1063–1095

Xiang H, Zhang L, Zhou H, Zhong Z, Zeng W, Liu R, Jin S (2008) U-Pb zircon geochronology and Hf isotope study of metamorphosed basic-ultrabasic rocks from metamorphic basement in southwestern Zhejiang: the response of the Cathaysia Block to Indosinian orogenic event. Sci China (Ser D) Earth Sci 51:788–800

Xu XS, Zhou XM, Wang DZ (1999) Crust-mantle interaction and the genesis of granite: a case study of coastal area of Southeastern China. Geol J China Univ 5(3):241–250 **(in Chinese with English abstract)**

Yang YQ, Ni YX, Guo YQ, Chou NM, Chen CH, Cai CF, Zhang YP, Liu JB, Chen YX (1987) Rock-forming and ore-forming characteristics of the Xikeng granitic pegmatites in Fujian Province. Miner Depos 6(3):10–21 **(in Chinese with English abstract)**

Yang JH, Wu FY, Chung SL, Wilde SA, Chu MF (2006) A hybrid origin for the Qianshan A-type granite, northeast China: geochemical and Sr–Nd–Hf isotopic evidence. Lithos 89(1–2):89–106

Yu JH, Zhou X, O'Reilly YS, Zhao L, Griffin WL, Wang R, Wang L, Chen X (2005) Formation history and protolith characteristics of granulite facies metamorphic rock in Central Cathaysia deduced from U–Pb and Lu–Hf isotopic studies of single zircon grains. Chin Sci Bull 50:2080–2089

Yu JH, O'Reilly SY, Zhao L, Griffin WL, Zhang M, Zhou X, Jiang SY, Wang LJ, Wang RC (2007) Origin and evolution of topaz-bearing granites from the Nanling Range, South China: a geochemical and Sr–Nd–Hf isotopic study. Mineral Petrol 90:271–300

Yu JH, Wang LJ, O'Reilly SY, Griffin WL, Zhang M, Li CZ, Shu LS (2009) A Paleoproterozoic orogeny recorded in a long-lived cratonic remnant (Wuyishan terrane), eastern Cathaysia Block, China. Precambrian Res 174(3–4):347–363

Yu JH, O'Reilly SY, Zhou MF, Griffin WL, Wang LJ (2012) U–Pb geochronology and Hf–Nd isotopic data from the Badu Complex, southeastern China: implications for the Precambrian crustal evolution and paleogeography of the Cathaysia Block. Precambr Res 222–223:424–449

Zeng W, Zhang L, Zhou HW, Zhong ZQ, Xiang H, Liu R, Jin S, Lu XQ, Li CZ (2008) Caledonian reworking of Paleoproterozoic basement in the Cathaysia Block: constraints from zircon U–Pb dating, Hf isotopes and trace elements. Chin Sci Bull 53(6):895–904

Zhang KJ (1997) North and South China collision along the eastern and southern North China margins. Tectonophysics 270(1–2):145–156

Zhang YQ, Xu XB, Jia D, Shu LS (2009) Deformation record of the change from Indosinian collision-related tectonic system to Yanshanian subduction-related tectonic system in South China during the Early Mesozoic. Earth Sci Front 16:234–247 **(in Chinese with English abstract)**

Zhang FF, Wang YJ, Chen XY, Fan WM, Zhang YH, Zhang AM (2011) Triassic high-strain shear zones in Hainan Island (South China) and their implications on the amalgamation of the Indochina and South China Blocks: Kinematic and $^{40}Ar/^{39}Ar$ geochronological constraints. Gondwana Res 19(4):910–925

Zhao KD, Jiang SY, Yang SY, Dai BZ, Lu JJ (2012) Mineral chemistry, trace elements and Sr–Nd–Hf isotope geochemistry and petrogenesis of Cailing and Furong granites and mafic enclaves from the Qitianling batholith in the Shi-Hang zone, South China. Gondwana Res 22:310–324

Zhao KD, Jiang SY, Chen WF, Chen PR, Ling HF (2013) Zircon U–Pb chronology and elemental and Sr–Nd–Hf isotope geochemistry of two Triassic A-type granites in South China: Implication for petrogenesis and Indosinian transtensional tectonism. Lithos 160–161:292–306

Zheng YF (2008) A perspective view on ultrahigh-pressure metamorphism and continental collision in the Dabie-Sulu orogenic belt. Chin Sci Bull 53(20):3081–3104

Zhou XM, Li WX (2000) Origin of late Mesozoic igneous rocks in Southeast China: implications for lithosphere subduction and underplating of mafic magmas. Tectonophysics 326:269–287

Zhou XM, Sun T, Shen WZ, Shu LS, Niu YL (2006) Petrogenesis of Mesozoic granitoids and volcanic rocks in South China: a response to tectonic evolution. Episodes 29(1):26–33

Zhu KY, Li ZX, Xu XS, Wilde SA (2013) Late triassic melting of a thickened crust in southeastern china: evidence for flat-slab subduction of the Paleo-Pacific plate. J Asian Earth Sci 74(18):265–279